

## Size and Depth Distributions of Nickel Nanoparticles in SiO<sub>2</sub> Fabricated by High-Flux Negative-Ion Implantation of 60 keV

H. Amekura, N. Umeda\*, Y. Takeda,  
H. Kitazawa and N. Kishimoto

Nanomaterials Laboratory, National Institute for Materials Science  
Fax: 81-298-59-5010, e-mail: AMEKURA.Hiroshi@nims.go.jp

\*Institute of Materials Science, University of Tsukuba  
Fax: 81-298-59-5010

Magnetic nanoparticles of nickel are fabricated in silica glasses (SiO<sub>2</sub>) using high-flux implantation of Ni negative-ions of 60 keV, without heat treatments. Temperature- and field- dependences of the magnetization show that the nanoparticles are in the superparamagnetic state with a blocking temperature of ~27 K. Cross-sectional transmission electron microscopy (XTEM) observation confirms nanoparticle formation in SiO<sub>2</sub>, with a mean diameter of 2.9 nm and the standard deviation of 1.0 nm. The depth distribution of implanted Ni ions in SiO<sub>2</sub> observed by XTEM is similar to the prediction of TRIDYN and SRIM2000 codes with taking account of the sputtering. The result indicates that the implanted Ni ions form nanoparticles at almost the same depths where the ions stopped, without long diffusional migration. This is contrast against the high-flux implantation of Cu negative-ions where distinct redistribution of the implanted ions is observed.

**Key words:** nanoparticle, superparamagnetism, TEM observation, negative-ion implantation, nickel, SiO<sub>2</sub>

### 1. INTRODUCTION

Metal nanoparticles dispersed in insulators draw much attention, because of applicability of optical switches [1] and single electron transistors [2], etc. Ferromagnetic nanoparticles are attractive for the super high-density data-storage application [3,4], etc. On the other hand, the superparamagnetic nanoparticles are applicable to the tunneling magnetic resistance (TMR) devices, etc [5]. Since not only the ion species but also the size and the size-distribution of nanoparticles determine magnetic properties of the nanoparticles, understanding of the relationship between the nano-scale structures and magnetic properties is required.

High-flux negative-ion implantation (HFNII) is one of the most promising methods to fabricate metal nanoparticles in insulators, without heat treatment, with good controllability inherent in ion implantation and without surface charging accumulation [6-9]. In fabrication of Cu nanoparticles in SiO<sub>2</sub>, control of the depth/size distribution is attained, to a certain extent, by changing ion flux [9]. Up to now, we have succeeded in fabricating Cu nanoparticles in amorphous SiO<sub>2</sub> and some other insulators [10,11], and in observing large optical nonlinearity [12], sub-pico seconds response [13] and single electron transport [14]. The HFNII method is applicable not only to Cu ions but also to other metal ions including magnetic ones. Recently we have applied the HFNII method to synthesis of Ni nanoparticles in SiO<sub>2</sub>, and have observed the superparamagnetic behaviors [15]. In this paper, morphology of the Ni nanoparticles is discussed using cross-sectional

transmission electron microscopy (XTEM) observation.

### 2. EXPERIMENTALS

Optical-grade silica glasses (KU-1: OH 820 ppm and other impurities 6.3 ppm) of 15 mm in diameter and 0.5 mm in thickness were implanted with Ni negative-ions of 60 keV from a Cs-assisted plasma-sputter type high-flux ion source [6]. The implanted area was 6 mm in diameter. The ion flux and the dose ranged over 1 - 100  $\mu\text{A}/\text{cm}^2$  and  $3 \times 10^{16}$  -  $1 \times 10^{17}$  ions/ $\text{cm}^2$ , respectively. The doses were confirmed by the Rutherford Backscattering Spectrometry (RBS) using 2.06 MeV He<sup>+</sup> beam. In this paper, results of a sample implanted with a flux of ~60  $\mu\text{A}/\text{cm}^2$  and a dose of  $\sim 4 \times 10^{16}$  ions/ $\text{cm}^2$  are mainly discussed. According to SRIM2000 code [16], the projectile range  $R_p$  and the straggling  $\Delta R_p$  of Ni ions of 60 keV are 47 nm and 16 nm in SiO<sub>2</sub>, respectively.

Cross-sectional transmission electron microscopy (XTEM) was conducted to evaluate micro- and nano-structures in the Ni-implanted region. After the Ni implantation, a thin Cr film of ~5 nm in thickness was deposited as a surface marker. The sample was sliced in cross-sectional direction, and thinned down to ~20  $\mu\text{m}$  using mechanical dimpling. Finally Ar ion milling of 3-5 kV attained a thin film for TEM. The acceleration voltage of TEM was 200 kV.

Optical transmission and reflection measurements were conducted in the wavelength range of 190-1700 nm at room temperature, using a dual-beam spectrometer with a resolution of 1 nm. The incident angles were 0

degrees for the transmission and 5 degrees for the reflection.

Effects of the heat treatments on the photo-absorption spectra were examined using a vacuum tube furnace at 1000 °C for 1hr. The base pressure was less than  $2 \times 10^{-3}$  Pa.

### 3. RESULTS AND DISCUSSION

#### 3.1 Morphology of Ni nanoparticles

Figure 1 shows a XTEM image of SiO<sub>2</sub> implanted with Ni negative-ions of 60 keV. Formation of the nanoparticles is clearly seen as black dots in Fig. 1. The projectile range  $R_p$  calculated by SRIM2000 code [16] is shown by a white bar. The largest particles locate around  $R_p$ . Smaller particles are observed in much shallower or much deeper regions than  $R_p$ .

The size distribution of the nanoparticles is plotted in Fig. 2. The mean diameter and the standard deviation are 2.9 nm and 1.0 nm, respectively. The nanoparticles larger than 6 nm or smaller than 1 nm are rarely observed. Although the lower limit of 1 nm is possibly due to the resolution of the observation, the higher limit of 6 nm is due to the kinetics of the nanoparticle formation.

The depth ( $X$ ) distribution of nanoparticle number density  $N(X)$  and Ni atomic concentration  $C(X)$  are shown in Fig. 3. The number density  $N(X)$  counts the nanoparticles, irrespective of the size. The Ni concentration  $C(X)$  counts the nanoparticles with taking the size, i.e., volume, into account. Although  $N(X)$  is almost flat from 10 nm to 80 nm as shown in Fig. 3,  $C(X)$  has a maximum from 30 to 50 nm. It indicates that larger particles locate in 30 - 50 nm deep, and smaller particles locate in 0 - 20 nm and 60 - 90 nm deep. The dependence is seen more clearly in Fig. 4, where the size distributions are shown in each depth layer of 10 nm thick. It is again noted that the larger particles locate around  $R_p$  where the Ni concentration is the higher. Smaller particles locate in the shallower or deeper regions where the Ni concentration is lower.

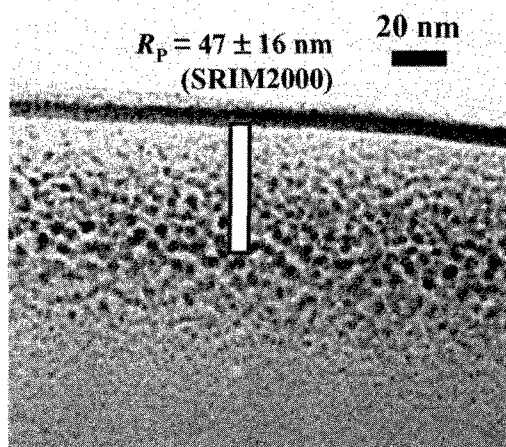


Fig.1 XTEM image of SiO<sub>2</sub> implanted with Ni negative-ions of 60 keV, at  $56 \mu\text{A}/\text{cm}^2$  to  $4 \times 10^{16}$  ions/cm<sup>2</sup>. The white bar indicates the projectile range  $R_p$  calculated by SRIM 2000 code. A black surface layer is a marker of Cr.

The observed  $C(X)$  is compared with calculated results from SRIM2000 [16] and TRIDYN [17] codes, as shown in Fig. 3. For fair comparison, we input the same values of parameters into both the codes, i.e., the surface binding energy, the bulk binding energy and displacement energy, etc, which were obtained from the data library included in SRIM2000. The experimental result is reproduced qualitatively with both the codes. However, the result is reproduced better with TRIDYN than SRIM2000. This fact indicates that the surface recession due to the sputtering is not serious, but cannot be neglected.

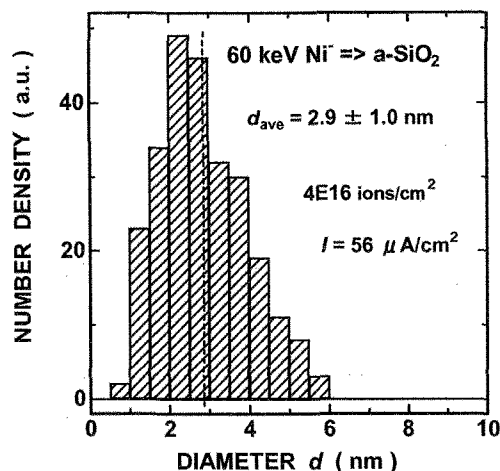


Fig. 2 Size distribution of Ni nanoparticles in SiO<sub>2</sub> implanted with Ni negative-ions of 60 keV, to  $4 \times 10^{16}$  ions/cm<sup>2</sup>.

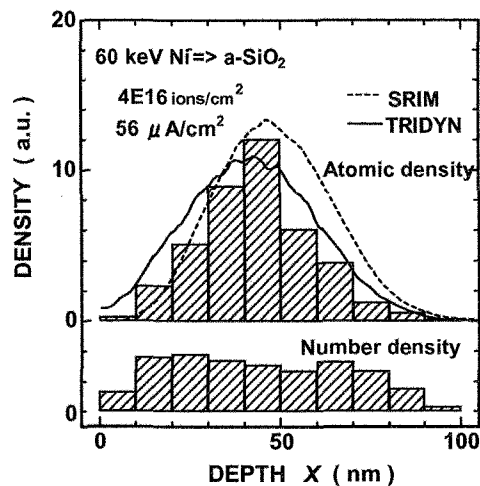


Fig. 3 Depth distribution of nanoparticles in SiO<sub>2</sub> implanted with Ni negative-ions of 60 keV to  $4 \times 10^{16}$  ions/cm<sup>2</sup>. The rectangles indicate the experimental results by XTEM observation. In the lower and upper parts, the number density of the nanoparticles and the Ni atomic concentration are shown, respectively. The broken and solid lines denote the distribution of Ni atoms calculated by SRIM2000 [16] and TRIDYN [17], respectively.

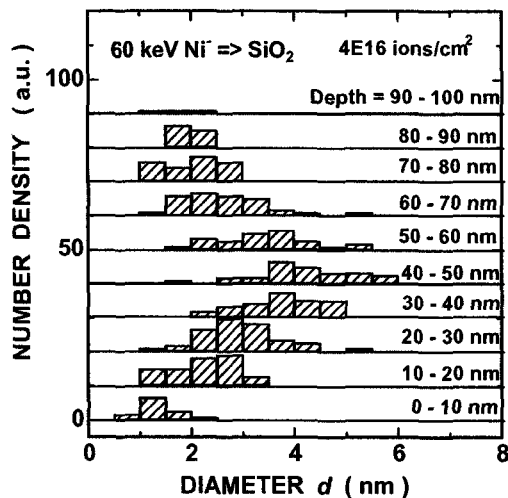


Fig. 4 Size distributions of Ni nanoparticles in equidistant depth layers of 10 nm in thickness each.

Roughly speaking, the depth distribution of nanoparticles is similar with the results of the projectile range calculation. This fact indicates that the implanted Ni ions form the nanoparticles at almost the same depths where the ions stopped, without long diffusional migration. This is contrast against the high-flux implantation of the Cu negative-ions where a distinct redistribution of the implanted ions is observed [9]. The difference is possibly due to diffusion constants of Cu and Ni under implantation. The diffusion constant of Cu may be larger than that of Ni under implantation. Even after the implantation, different diffusion behaviors are visible in annealing effect on optical spectra.

### 3.2 Thermal stability of Ni nanoparticles

Figure 5 shows the optical transmission spectra of SiO<sub>2</sub> implanted with 60 keV negative-ions of Ni (upper half) and Cu (lower half), both in the as-implanted state and after annealing in vacuum at 1000 °C for 1 hr. In the as-implanted states, the spectra are well explained with formation of Ni and Cu nanoparticles and defects in SiO<sub>2</sub> [12,15].

In the case of Cu implanted SiO<sub>2</sub> after 1000 °C annealing, all the absorption disappeared. It indicates that all the Cu nanoparticles were dissolved by thermally-enhanced diffusion, and most of Cu atoms probably escaped from the SiO<sub>2</sub> surface to outside [18]. If the Cu atoms stay inside as isolated atoms in SiO<sub>2</sub>, the strong broad absorption is expected at photon energy larger than ~4 eV [19]. From the spectrum shown in Fig. 5, the existence of the isolated Cu atoms in SiO<sub>2</sub> is excluded.

In the case of Ni implanted SiO<sub>2</sub> after 1000 °C annealing, the absorption slightly decreases. It is noted that the decrease around 6 eV is due to a recovery of defects in SiO<sub>2</sub>, probably E' centers [15]. A little portion of Ni nanoparticles was lost after the annealing. A preliminary RBS result shows the same conclusion.

Probably the diffusion constant of Ni is smaller than

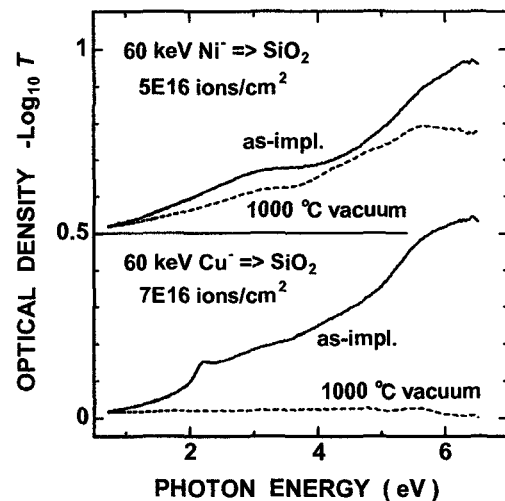


Fig. 5 The optical transmission spectra of silica glasses implanted with 60 keV negative-ions of Ni (upper half) and Cu (lower half), in as-implanted states and after the vacuum annealing at 1000 °C.

that of Cu, or the nanoparticle formation energy of Ni is larger than that of Cu. The difference maybe explains the different morphology and depth distribution of nanoparticles between Ni and Cu under the high-flux implantation. Similarly, the redistribution of implanted Cu atoms under the implantation is easier than that of Ni atoms.

### 3.3 The nanoparticle size and the superparamagnetism

From the blocking temperature  $T_B$  of superparamagnetic particles observed by SQUID magnetometer, the diameter  $d_c$  of the magnetic nanoparticles is estimated as,

$$V_c = \frac{4\pi}{3} \left( \frac{d_c}{2} \right)^3 = 25.3 \frac{k_B T_B}{K} \quad (1)$$

where  $V_c$ ,  $k_B$  and  $K$  denote the volume of the superparamagnetic nanoparticle, the Boltzman constant and the magnetic anisotropy constant, respectively [20]. As for the mean  $T_B$  value of the nanoparticle ensemble, the peak temperature of the zero-field magnetization is used, i.e., ~27 K in this case [15]. It should be noted that the  $K$  value for eq. (1) of Ni nanoparticles could not be approximated by the value at room temperature, because of the large temperature dependence. It is contrast with Fe and Co where the temperature dependence is small [21]. If the  $K$  value is approximated by the value of the bulk Ni, i.e.,  $\sim 1.2 \times 10^5$  J/cm<sup>3</sup> at ~5 K [23], the magnetic mean diameter of ~5 nm is obtained. It should be noted again that the mean diameter observed by TEM is 2.9 nm. One might explain the difference assuming that only larger nanoparticles than, say, 4.5 nm in diameter, contributed to the magnetization. So larger magnetic diameter could be obtained. However, as shown in Fig. 2, only small portion of nanoparticles is larger than 4.5 nm. This is inconsistent with relatively large magnetization observed [15]. In stead, the difference is explained by an

enhancement of the  $K$  value due to the nano-sized effect, which was reported in Ni-Co nanoparticles [22].

#### 4. CONCLUSIONS

The superparamagnetic Ni nanoparticles are fabricated in silica glasses using high-flux implantation of nickel negative-ions of 60 keV. The XTEM observation and the photo-absorption measurements confirm the formation of metallic Ni nanoparticles with the mean diameter of 2.9 nm and the standard deviation of 1.0 nm. The depth distribution of Ni atoms is similar to those predicted by the projectile-range calculations. It indicates that the implanted ions form the nanoparticles at almost the same depths where the ions stopped, without long diffusional migration. The larger nanoparticles are observed at the depth where the Ni concentration is the higher. This is contrast with the SiO<sub>2</sub> implanted with Cu under almost the same implantation conditions, where the large redistribution of depth profile is observed. The difference may relate to the behaviors of the nanoparticles after annealing in vacuum at 1000 °C. While the Cu nanoparticles disappear, the Ni nanoparticles still survive. The nanoparticle diameter estimated from the superparamagnetic blocking temperature, using the bulk magnetic anisotropy constant  $K$ , was  $\sim 5$  nm, i.e., larger than the observed value by TEM, 2.9 nm. The difference may indicate the enhanced magnetic anisotropy constant  $K$  due to the nano-sized effect.

#### ACKNOWLEDGMENTS

The authors express their thanks to Ms. J. Lu (NIMS) for assistance of TEM sample preparation. A part of this study was financially supported by the Budget for Nuclear Research of the MEXT, based on the screening and counseling by the Atomic Energy Commission.

#### REFERENCES

- [1] R.F. Haglund, L. Yang, R.H. Magruder, C.W. White, R.A. Zhur, L. Yang, R. Dorsinville and R.R. Alfano, *Nucl. Instr. and Meth.*, **B91**, 493-504 (1994).
- [2] A. Nakajima, H. Nakao, H. Ueno, T. Futatsugi and N. Yokoyama, *Appl. Phys. Lett.*, **73**, 1071-1073 (1998).
- [3] D. Kumar, H. Zhou, T.K. Nath, A.V. Kvit and J. Narayan, *Appl. Phys. Lett.*, **79**, 2817-2819 (2001).
- [4] M. Klimenkov, J.von Borany, W. Matz, D. Eckert, M. Wolf and K.-H. Muller, *Appl. Phys.*, **A74**, 571-575 (2002).
- [5] J.I. Gittleman, Y. Goldstein and S. Bozowski, *Phys. Rev.*, **B5**, 3609-3621 (1972).
- [6] Y. Mori, G.D. Alton, A. Takagi, A. Ueno and S. Fukumoto, *Nucl. Instr. and Meth.*, **A273**, 5-12 (1988).
- [7] J. Ishikawa, H. Tsuji, Y. Toyota, Y. Gotoh, K. Matsuda, M. Tanjyo and S. Sakaki, *Nucl. Instr. and Meth.*, **B96**, 7-12 (1995).
- [8] N. Kishimoto, Y. Takeda, V.T. Gritsyna, E. Iwamoto and T. Saito, "IEEE Transactions from 1998 International Conference on Ion Implantation Technology Proceedings", Ed. By J. Matsuo, G. Takaoka and I. Yamada, IEEE, Piscataway (1999) pp. 342-345.
- [9] N. Kishimoto, N. Umeda, Y. Takeda, V.T. Gritsyna, T.J. Renk and M.O. Thompson, *Vacuum*, **58**, 60-78 (2000).
- [10] N. Kishimoto, Y. Takeda, N. Umeda, V.T. Gritsyna, C.G. Lee and T. Saito, *Nucl. Instr. and Meth.*, **B166-167**, 877-881 (2000).
- [11] Y. Takeda, C.G. Lee and N. Kishimoto, *Nucl. Instr. and Meth.*, **B191**, 422-427 (2002).
- [12] Y. Takeda, V.T. Gritsyna, N. Umeda, C.G. Lee and N. Kishimoto, *Nucl. Instr. and Meth.*, **B148**, 1029-1033 (1999).
- [13] Y. Takeda, J.P. Zhao, C.G. Lee, V.T. Gritsyna and N. Kishimoto, *Nucl. Instr. and Meth.*, **B166-167**, 877-881 (2000).
- [14] H. Amekura, N. Umeda, Y. Takeda, N. Kishimoto and H. Nejo, "Proceedings of the 5<sup>th</sup> International Symposium on Advanced Physical Fields (APF-5)", Ed. by K. Yoshihara, NRIM, Tsukuba (2000) pp. 203-207.
- [15] H. Amekura, H. Kitazawa, N. Umeda, Y. Takeda and N. Kishimoto, "Proceedings of SPIE" Vol. 4936 (2002) pp. 1-8.
- [16] J.F. Ziegler, J.P. Biersack and U. Littmark, "The Stopping and Range of Ions in Solids", Pergamon press, New York (1985) Chap.8. <http://www.srim.org/>.
- [17] W. Moeller and W. Eckstein, *Nucl. Instr. and Meth.*, **B2**, 814-818 (1984).
- [18] N. Umeda, N. Kishimoto, Y. Takeda, C.G. Lee and V.T. Gritsyna, *Nucl. Instr. and Meth.*, **B166-167**, 864-870 (2000).
- [19] K. Fukumi, A. Chayahara, K. Ohora, N. Kitamura, Y. Horino, K. Fujii, M. Makihara, J. Hayakaya and N. Ohno, *Nucl. Instr. and Meth.*, **B149**, 77-80 (1999).
- [20] For example, M. Solzi, M. Ghidini and G. Asti, "Magnetic Nanostructures", Ed. by H.S. Nalwa, American Science Pub., (2002) Chap.4.
- [21] E.P. Wohlfarth, "Ferromagnetic Materials", Ed. by E.P. Wohlfarth, North-Holland Pub., Amsterdam (1980) pp. 1-70.
- [22] C. de Julian, C. Sangregorio, G. Mattei, G. Battaglin, E. Cattaruzza, F. Gonella, S. Lo Russo, F. D'Orazio, F. Lucari, G. De, D. Gatteschi and P. Mozzoldi, *J. Magn. Magn. Mater.*, **226-230**, 1912-1914 (2001).

(Received December 21, 2002; Accepted March 26, 2003)